DALHOUSIE UNIVERSITY

Surface Adsorption from the Exchange-Hole Dipole Moment Dispersion Model

Matthew S. Christian,*,† A. Otero-de-la-Roza,*,‡ and Erin R. Johnson*,†

Department of Chemistry, Dalhousie University, 6274 Coburg Road, Halifax, Nova Scotia, Canada B3H 4R2, and Department of Chemistry, University of British Columbia, Okanagan, 3247 University Way, Kelowna, British Columbia, Canada V1V 1V7.

E-mail: mchristian@dal.ca; aoterodelaroza@gmail.com; erin.johnson@dal.ca

Abstract

The accurate calculation of intermolecular interaction energies with density-functional theory (DFT) requires methods that include a treatment of long-range, non-local dispersion correlation. In this work, we explore the ability of the exchange-hole dipole moment (XDM) dispersion correction to model molecular surface adsorption. Adsorption energies are calculated for six small aromatic molecules (benzene, furan, pyridine, thiophene, thiophenol, and benzenediamine) and the four DNA nucleobases (adenine, thymine, guanine, and cytosine) on the (111) surfaces of the three coinage metals (copper, silver, and gold). For benzene, where the experimental reference data is most precise, the mean absolute error in the computed absorption energies is 0.04 eV. For the other aromatic molecules, the computed binding energies are found to be within 0.09 eV of the available reference data, on average, which is well below the expected experimental uncertainties for temperature-programmed desorption measurements. Unlike other dispersion-corrected functionals, adequate performance does not require changes to the canonical XDM implementation, and the good performance of XDM is explained in terms of the behaviour of the exchange hole. Additionally, the base functional employed (B86bPBE) is also optimal for molecular studies, making B86bPBE-XDM an excellent candidate for studying chemistry on material surfaces. Finally, the non-covalent interaction (NCI) plot technique is shown to detect adsorption effects in real space on the order of tenths of an eV.

1 Introduction

Molecule-surface interactions influence all processes that occur on a the surface of a material. Modeling these interactions accurately is important in the study of topics as diverse as monolayer formation on metal surfaces,[1] construction of DNA microarrays,[2] molecular electronics,[3] and heterogeneous catalysis.[4] Molecular adsorption has been traditionally classified as a) chemisorption, which is relatively strong and where covalent interactions between molecule and substrate are predominant, and b) physisorption, which is dominated by weak non-covalent interactions. Chemisorption and physisorption also differ in the extent to which the electronic structure of molecule and surface are disrupted at the adsorbed geometry. Chemisorption perturbs the surface band structure as well as the electronic energy levels of the adsorbate, whereas physisorption occurs through long-range effects that have little impact on the electronic levels. The nature of an adsorption event (chemisorption or physisorption) depends on the properties of

*To whom correspondence should be addressed
†Dalhousie University
‡University of British Columbia, Okanagan

both the molecule and surface. Simple aromatic molecules, such as benzene, thiophene, and pyridine are known to physisorb on noble-metal surfaces.[5–11]

Since long-range effects are essential to describe molecule-surface interactions, it is critical to have an accurate representation of dispersion forces when modeling physisorption and, to a lesser extent, chemisorption phenomena.[12,13] If dispersion models are included, quantum-chemical methods can be applied to complex systems, such as predicting polymorphic self-assembled monolayer structures in good agreement with experimental results.[14,15]

Accurately predicting physisorption geometries and energies with density-functional theory (DFT) is challenging because conventional functionals do not account for London dispersion interactions.[16,17] Indeed, previous physisorption studies using non-dispersion-corrected functionals yielded drastically underestimated adsorption energies, relative to experiment.[18–20] The addition of a dispersion correction greatly increases the accuracy. Several recent studies have modeled physisorption with an assortment of dispersion-corrected functionals, including pairwise,[20–28] many-body[29] and non-local[26,28,30–33] dispersion corrections. The majority of these studies focused on the adsorption of benzene on noble metals – copper, silver, and gold.[21–28,30,32,33]

Computational methods provide more detailed information regarding the nature of individual molecular-surface interactions than can be determined from experiments, which are complicated by differing molecule-surface interaction orientations, monolayer formation, and surface defects. Experimentally, molecular adsorption energies are generally measured via temperature-programmed desorption (TPD) analysis. The desorption energy is determined from the temperature of maximum desorption via Redhead's analysis.[34,35] This procedure is appropriate in the zero-coverage limit and where monolayers involve only weak intermolecular interactions. Since Redhead's analysis only accounts for intermolecular interactions through the pre-exponential factor, results can differ from actual adsorption energies.[36] In the particular case of benzene on coinage metals, Liu *et. al*[29] recently determined the adsorption energy of benzene using the complete analysis method, which is expected to be more accurate than the Redhead model. Benzene also does not have a coverage-dependent molecule-surface orientation below monolayer coverage. Hence, benzene on coinage metals is an excellent system to conduct benchmarking calculations of dispersion-corrected density functionals.

In this work, we present the first comprehensive performance study of the exchange-hole dipole moment (XDM) dispersion model[37] applied to molecular surface adsorption. XDM models the dispersion energy as a sum over all pairwise atomic interactions, with non-empirical, density-dependent dispersion coefficients, involving C_6, C_8, and C_{10} terms. When paired with suitable base density functionals, XDM has been demonstrated to be highly accurate for molecular dimers,[38] molecular crystals,[39] and graphene,[40] as well as for metallophilic interactions,[41] without any system-specific re-parameterization. A study similar to this work was conducted by Chwee and Sullivan[24] for benzene on noble-metal surfaces,[24] where the authors successfully used a modification of XDM involving only the C_6 and C_8 terms, to calculate adsorption energies for benzene on noble metals. While their results show that XDM predicts suitable physisorption energies, the damping parameters used were taken from earlier work involving post-Hartree-Fock calculations[42] and are not expected to be generally applicable. In addition, several ad-hoc modifications to the XDM method were used.

Previous works have suggested that simple pairwise methods[21,22] are not suitable for accurate calculation of physisorbed energies.[25–29] In this article, the canonical XDM implementation with the usual damping function parameters (determined for gas-phase dimers[38,40]) is used to demonstrate that a pairwise dispersion correction does not only represent molecule-surface interactions accurately, but it does so to an accuracy on par with previous estimates using either more complex dispersion corrections (including many-body effects) or purposely-built

methods for molecule-surface interactions, such as vdW-TS^{surf},[25,28] and at a computational cost that is comparable to a semilocal DFT calculation. The nature of the molecule-surface interactions is further analyzed using non-covalent interaction (NCI) plots,[43,44] where we demonstrate that NCI detects the minute energetic binding effects between molecule and substrate in real space. This paper confirms that physisorption energies can be accurately calculated using the XDM dispersion model for single-molecule adsorption and that XDM is an excellent model for modeling chemical processes on material surfaces.

2 Computational Methods

Copper, silver, and gold (111) surfaces were modeled using (4×4) super-cells. The model surfaces were four atomic layers thick and a vacuum of 25 Å was inserted between each slab. The atomic positions of the two bottom layers were held fixed while the top two layers were allowed to relax. Our molecular test set consisted of ten small aromatic molecules, including the four DNA nucleobases: benzene, furan, pyridine, thiophene, thiophenol, 1,4-benzenediamine (BDA), adenine, cytosine, guanine, and thymine. Each molecule was initially placed roughly 3 Å above the surface in a parallel position such that the aromatic region was centered over a surface atom and the geometry optimized. Additional calculations were performed for furan, pyridine, thiophene, and thiophenol, with the molecule initially placed perpendicular to the surface, such that the heteroatom was directly above a surface atom.

Periodic-boundary DFT calculations were performed using the pseudopotential/plane-wave approach and the Projector Augmented Wave formalism.[45] Calculations were carried out using Quantum ESPRESSO[40,46] version 5.3.0 with the B86b[47] exchange functional and PBE[48] correlation, known to perform well in conjunction with XDM.[39] Additional XDM calculations with the PBE exchange-correlation functional[48] were performed for benzene adsorbed on the three metal surfaces for comparison with other literature results. PAW datasets from the Quantum ESPRESSO pslibrary are used in all cases. The calculations used a 2×2×1 Γ-centered **k**-point grid, a plane-wave cutoff of 50 Ry and a density-expansion cutoff of 400 Ry, and cold smearing,[49] with a smearing parameter of 0.01 Ry. Subsequent single-point energy calculations with 4×4×1 **k**-points, as well as higher plane-wave and density-expansion cut-offs of 60 and 800 Ry respectively, were performed at the relaxed geometries. Results of convergence tests, with respect to the number of metal layers, **k**-point grid, and plane-wave cut-off are reported in the Supporting Information (SI).

The XDM dispersion functional is a post-SCF correction to the base DFT energy, calculated using one of the usual semilocal functionals:

$$E = E_{\text{base}} + E_{\text{XDM}} \tag{1}$$

$$E_{\text{XDM}} = -\sum_{n=6,8,10}\sum_{i<j}\frac{C_{n,ij}f_n(R_{ij})}{R_{ij}^n} \tag{2}$$

In this equation, the sum runs over all pairs of atoms i and j in the system. R_{ij} is the interatomic distance, f_n is a damping function that reduces the dispersion correction at short range, and the $C_{n,ij}$ are pairwise dispersion coefficients. In the XDM model, each $C_{n,ij}$ is approximated non-empirically via second-order perturbation theory using the multipole moments of a reference electron and its exchange hole and atom-in-molecule polarizabilities for the interacting atoms.[37] The XDM dispersion model offers excellent accuracy for both gas-phase[38] and condensed-matter[39,40] systems, notably including the interactions between noble-metal complexes.[41]

The adsorption energy is defined as the difference between the calculated energy of the adsorbed molecule and the energies of the bare surface and isolated molecule:

$$E_{\text{adsorption}} = E_{\text{surf}} + E_{\text{molec}} - E_{\text{complex}} \tag{3}$$

The contributions of image interactions[32] on E_{molec}, arising from the use of periodic boundary conditions, were evaluated by calculating the molecular energy in two configura-

tions. First, energies were calculated for each molecule in a large vacuum to nullify any self-interactions. Second, E_{molec} was calculated for an isolated molecule in a cell with the same dimensions as the surface unit cell. The results are compared in the Supporting Information. For the six small aromatic molecules, the energy differences between these two definitions were negligible, with the largest variations of 0.03 eV occurring for thiophene and 1,4-benzenediamine (cis). However, image interactions for the nucleobases were found to be as large as 0.10 eV, due to their greater molecular sizes and polarities. In order to eliminate the effect of these image interactions, all adsorption-energy results are reported relative to a periodic array of molecules with the same cell dimensions as for the physisorbed complex.

Non-covalent interaction (NCI)[43,44] plots at the optimized adsorption geometry were generated using the Critic2 program[50] to investigate the nature of the interactions between the physisorbed molecules and the metal surfaces. The NCI index reveals non-covalent contacts based on the electron density and the reduced density gradient (RDG) defined as:

$$s = \frac{1}{2(3\pi^2)^{1/3}} \frac{|\nabla\rho|}{\rho^{4/3}} \tag{4}$$

This approach provides qualitative information about the presence and extent of non-bonded atomic contacts using isosurfaces of the RDG. These isosurfaces are defined to enclose regions with low density and low RDG that are a signature of non-covalent interactions.[43] Weak dispersion interactions typically appear as broad, green isosurfaces, while stronger directional non-covalent interactions (such as hydrogen bonds) appear as localized blue domains.

3 Results and Discussion

3.1 Benzene

Because abundant theoretical predictions and highly-precise experimental adsorption-energy results[29] are available, we focus first on the adsorption of benzene on the three metal surfaces. From the B86bPBE-XDM calculations, the benzene molecule adsorbs roughly parallel to the surface and the equilibrium distances between the nearest atoms in the benzene molecule and the metal surface are 2.71, 3.03, and 3.15 Å for copper, silver, and gold, respectively. The benzene-silver distance is in good agreement with the only available experimental measurement of 3.04±0.02 Å.[29] Table 1 compares our calculated adsorption energies with results from other dispersion methods in the literature, and with experimental results using complete analysis.[29]

In agreement with previous studies,[18–20] the PBE functional without any dispersion correction, predicts only extremely weak physisorption, with adsorption energies around 0.1 eV, compared to the experimental values of 0.65–0.69 eV. Among the dispersion corrected functionals, the DFT-D2 dispersion correction to PBE causes an overestimation of the adsorption energies, particularly for benzene on gold.[21] This overestimation is likely due to a combination of the use of empirically-derived C_6 dispersion coefficients for the metal atoms (which in PBE-D2 are independent of the chemical environment) and, perhaps, to the omission of higher-order C_8 and C_{10} terms.

The more sophisticated DFT-D3 dispersion correction, in which the dispersion coefficients do depend on the adsorption geometry, shows improvement over D2, with a mean absolute error (MAE) of 0.19 eV. PBE-D3 improves upon PBE-D2 for silver[22] and gold,[23] but severely overestimates the adsorption energy for benzene on copper.[23] It has been argued that the overestimation of dispersion coefficients for metals with D3 may be due to the use of neutral hydrides with various coordination numbers as model systems and that improved coefficients for metals could be improved by changing the choice of reference.[51] The PBE-D3 result is further improved if a 3-body dispersion term is included, since the 3-body term is repulsive and serves to off-set the over-binding.[23]

The Tkatchenko-Scheffler (TS) dispersion method[52] also strongly overestimates adsorption of benzene to metals,[25,28] likely due to

Table 1: Comparison of reported adsorption energies for benzene on noble-metal surfaces in eV. The combination of base density functional and dispersion correction are noted in each case. The mean absolute error (MAE) is computed for the functionals for which the three adsorption energies have been reported.

Base Functional	Disp. Method	Cu	Ag	Au	MAE	Ref.
PBE	none	0.08	0.08, 0.09	0.08, 0.15	0.57–0.59	25,28
PBE	D2	0.86	—	1.35	—	21
PBE	D3	0.99	0.74	0.86	0.19	23
PBE	D3(ABC)	0.79	0.61	0.73	0.08	23
PBE	vdW-TS	1.02, 1.07	0.82, 0.87	0.80, 0.84	0.20–0.25	25,28
PBE	vdW-TS^{surf}	0.79, 0.86	0.73, 0.75	0.73, 0.74	0.08–0.11	25,28
PBE	MBD	0.63	0.57	0.56	0.09	29
HSE	MBD	0.78	0.68	0.67	0.04	29
opt-B86b	vdw-DF	0.82	0.76	0.86	0.14	30
opt-B88	vdw-DF	0.74	0.72	0.82	0.09	30
opt-PBE	vdw-DF	0.68	0.71	0.71	0.03	30
revPBE	vdw-DF	0.53	0.55	0.56	0.13	30
rPW86	vdw-DF	0.49	0.52	0.55	0.15	30
SCAN	rVV10	0.74	0.68	0.73	0.04	33
PBE	XDM	0.54	0.58	0.61	0.10	This work
B86bPBE	XDM	0.59	0.68	0.64	0.04	This work
Expt.		0.69±0.04	0.68±0.05	0.65±0.03		29

the free-metal-atom reference for the dispersion coefficients. A version of the TS method specifically designed for surfaces has been proposed[27] that recovers the C_3 dispersion coefficient for the metal surface.[53] In practice, this is achieved by scaling the dispersion coefficients, resulting in lower adsorption energies with a MAE of around 0.1 eV compared to the experimental values. The newer many-body dispersion (MBD) modification to the original TS method[54,55] accurately predicts the adsorption energies for benzene on the noble metals,[29] giving a mean absolute error of only 0.04 eV when combined with the range-separated hybrid functional HSE (which is considerably more computationally expensive than PBE).

Non-local van der Waals functionals[56,57] provide an alternative, non-empirical approach to model dispersion. Non-local functionals of the vdw-DF type display good performance for determining adsorption energies of benzene on noble metals.[28,30,32] While there is significant spread of the vdW-DF results depending on the choice of base functional, opt-B88, opt-PBE, and revPBE offer good agreement with experiment and all predict effectively degenerate adsorption energies for the three surfaces, in agreement with experimental observations. The performance of opt-PBE is particularly good with a mean absolute error of only 0.03 eV, within the precision of the experimental data. The SCAN meta-GGA combined with the non-local rVV10 dispersion correction[33] also performs quite well, with a MAE of 0.04 eV, again comparable to the experimental precision.

The adsorption energies calculated with XDM are generally lower than the other pairwise dispersion corrections. The adsorption energies are found to be nearly degenerate down the group, in agreement with the vdW-TS^{surf} and MBD results. The B86bPBE functional provides better performance when paired with XDM than does the PBE functional, in agreement with previous work.[39] This is to be expected given the improved behaviour of the

B86b exchange enhancement factor in the large reduced-gradient limit.[40,47,58] With a MAE of 0.04 eV, the B86bPBE-XDM adsorption energies are in comparable agreement with experiment as those obtained with the more computationally expensive HSE-MBD. B86bPBE-XDM also yields lower errors relative to vdW-TS$^{\text{surf}}$ and the vdw-DF functionals, except for opt-PBE, which shows superior performance.

It should be noted that the combination of B86bPBE and XDM performs well for physisorption without any modification or reparameterization of the dispersion model and that the same functional has been shown to give accurate results for lattice energies of molecular crystals[40] and other non-covalently bound materials.[37] Hence, B86bPBE is a good candidate functional when adsorption on material surfaces is only one aspect of the system under study and a good representation of interactions between molecules on the surface is also necessary (e.g. heterogeneous catalysis, self-assembled monolayers, etc.).

3.2 Dispersion coefficients: the role of the exchange-hole dipole moment

In this section, we consider why the XDM model is capable of providing an improved treatment of surface adsorption relative to other pairwise dispersion corrections. In XDM, the C_6 (and higher-order) dispersion coefficients are determined from the atomic polarizabilities and integrals involving the exchange-hole dipole moment. Specifically, for a homonuclear pair of atoms, the C_6 dispersion coefficient is

$$C_{6,ii} = \frac{1}{2}\alpha_i \langle M_1^2 \rangle_i \tag{5}$$

where

$$\langle M_1^2 \rangle_i = \sum_\sigma \int w_i(\boldsymbol{r}) \rho_\sigma(\boldsymbol{r}) \left[r - (r - d_{X\sigma})\right]^2 d\boldsymbol{r}. \tag{6}$$

In these equations, $w_i(\boldsymbol{r})$ are the Hirsfeld partitioning weights;[59] $d_{X\sigma}$ is the dipole moment between the reference electron and its corresponding exchange hole, evaluated using the Becke-Roussel model;[60] and α_i is the atomic polarizability, evaluated by a volume scaling of the reference free-atomic polarizabilities.[61] Both the atomic polarizabilities and moment integrals show considerable dependence on the atomic environment, resulting in highly variable values for the dispersion coefficients.[62]

Table 2 shows the free-atom polarizibilities, as well as the dipole moment integrals and homonuclear dispersion coefficients for copper, silver, and gold. Values are reported for the free atoms, bulk metal, and surface, taken as the atoms in the top layer in the bare slab model used in the adsorption calculations. Literature C_6 values from the vdW-TS$^{\text{surf}}$ model[27] are also given for comparison.

The tabulated data shows that silver is more polarizable than copper and gold and therefore has larger dispersion coefficients. Relativistic effects increase the electronegativity of gold,[41] decreasing its polarizability, and causing it to have dispersion coefficients closer to those of copper than silver.

The dispersion coefficients decrease considerably (by nearly a factor of one half) going from the free atoms to the surface and bulk metal. This explains the over-binding tendency of other pairwise dispersion corrections (Table 1), which do not capture this large decrease in C_6 for the bulk metals. The decrease is not due to changes in the atomic volumes, which vary by less than 10%. Rather, Table 2 reveals that the difference in the dispersion coefficients originates from the exchange-hole dipole moment integrals.

The finding that the atomic volumes remain nearly constant for each element, means that the atomic polarizabilities are relatively independent of the atomic environment. This is not what is seen in the vdW-TS^{surf} method,[27] where the effective 'atom-in-a-solid' polarizabilities are much smaller than for the corresponding free atoms. Nevertheless, both approaches give similar bulk C_6's for gold, although in the case of XDM the variation from the free-atom value arises from a change in the exchange-hole dipole moment, rather than the polarizability.

The variation in the moment integrals can be easily understood by considering the nature of

Table 2: Free-atomic polarizabilities (α, in Å^3) for copper, silver, and gold. Also shown are the $\langle M_1^2 \rangle$ moments and the homoatomic C_6 dispersion coefficients (in atomic units) obtained for the bulk metal, the bulk metal chloride (MCl, in its fcc structure), the top layer of the metal surface, and the free atoms with XDM. The dispersion coefficients are compared with literature values for the bulk metal and free atoms from the vdW-TS^{surf} model.[27]

Metal	α	$\langle M_1^2 \rangle$ XDM				C_6 XDM				C_6 vdW-TS	
	free	bulk metal	bulk MCl	surf	free	bulk metal	bulk MCl	surf	free	bulk metal	free
Cu	6.2	5.27	6.82	6.19	9.71	103	130	120	180	59	253
Ag	7.2	7.30	9.79	9.19	15.64	179	226	221	351	122	339
Au	5.8	6.43	9.28	8.70	13.86	137	182	170	271	134	298

the exchange hole in the valence region of a free atom compared to a bulk metal. In the free atom, the electron density decays exponentially and exchange hole will remain centered on the atom, even when the reference electron is relatively far from the nucleus.[60] This results in large values of the exchange-hole dipole moment. Conversely, the electron density between two atoms in a metal remains quite flat[63] causing the exchange hole to be centered very near the position of the reference electron.[60] Indeed, for a uniform electron gas, the exchange hole is centered exactly at the reference point. This results in small values of the exchange hole dipole moment.

Table 2 also shows the calculated moments and coefficients for the metal in the rocksalt-type phase of the bulk metal chloride MCl (M = Cu, Ag, Au). This phase is the experimentally-observed structure of AgCl, and a metastable phase in AuCl and CuCl, and has been used in the past to explore the importance of metallophilic interactions in simple solids.[41] It is interesting to note that the crystallographic positions of the metal atoms are the same in the chloride as in the elemental metal. The critical influence of the atomic environment on the XDM moments, and hence on the dispersion coefficients, is clearly exemplified by comparing the elemental metals with the corresponding chlorides. The atomic volumes in the metal are larger than in the chloride (e.g. 128.5 bohr^3 in AuCl compared to 136.3 in Au metal). However, the XDM moments are smaller in the metal, because the exchange-hole dipole is significantly smaller and, in consequence, the metallic dispersion coefficients are lower.

We note that pairwise dispersion correction methods such as DFT-D2 and the original Tkatchenko-Scheffler model, which depend on reference free-atom dispersion coefficients will be unable to predict a greatly reduced C_6 for the bulk metal. The necessary physics to describe this variation in the dispersion coefficients is captured by the behaviour of the exchange hole, but not by a simple volume scaling.

3.3 Comparison to other experimental and theoretical adsorption energies

Table 3: Comparison of calculated adsorption energies (in eV) with available experimental data for selected molecules on copper, silver, and gold surfaces.

Molecule	Metal	Calc.	Expt.
Thiophene	Cu	0.66	0.66[6]
Thiophene	Ag	0.67	0.52[7]
Thiophene	Au	0.62	0.68[8]
Furan	Cu	0.53	0.43[9]
Pyridine	Cu	0.69, 0.86	0.53, 0.84[10]
1,4-BDA	Au	1.12	1.0[11]
MAE		0.09	

Table 3 shows a comparison of B86bPBE-XDM results with experimental TPD adsorption energies, where available. With the excep-

tion of the complete analysis results for benzene,[29] discussed previously, all of the TPD reference data will have fairly low precision. This occurs because the conversion of the temperature of maximum desorption to a desorption energy uses an empirically-chosen pre-exponential factor, typically taken to be 10^{13}/s.[34] Coverage dependence of the pre-exponential factor[36] can introduce uncertainties of up to 0.2 eV for the molecules considered here. Additionally, some heteroaromatic molecules can adsorb in multiple stable configurations, resulting in a range of measured physisorption energies from TPD. For pyridine, the two reported experimental values[10] were compared with the computational results for the parallel and perpendicular orientations. The mean absolute error (MAE) is 0.09 eV, showing that the XDM results agree with the reference values to within the expected experimental precision.

The case of 1,4-benzenediamine (BDA) on gold has also been studied using a vdw-DF functional by Li et al.[64] and will be discussed in more detail. For this system, an experimental adsorption energy of 1 eV was measured using temperature-dependent helium atom scattering.[11] BDA can adsorb to coinage metals in two geometries, where the amine groups on both sides of the phenyl ring are in relative *cis* and *trans* positions. Our calculated adsorption energies are 1.10 eV for *cis* and 1.12 eV for *trans* and both values are in good agreement with the experimental result. For comparison, PBE-vdW-DF gives 0.94 eV for the *trans* and 0.98 eV for the *cis* orientations,[64] closely matching our results and experiment. For the trans orientation, the tilt angle is predicted to be 8.4° with B86bPBE-XDM, in agreement with the optimal tilt angle of 8° found with PBE-vdW-DF.[64] This is significantly smaller than the angle of ca. 35° obtained with PBE in the absence of a dispersion correction.[64] Thus, dispersion causes the trans form of BDA to lie flatter on the surface. Interestingly, the "weak but non-negligible amine-Au bond" observed in previous studies[11,64] is revealed by an increased energetic contribution from the base functional in the *trans* configuration (Table 4) and also by the blue domains shown by the NCI plots in Figure 1. This same chemisorption effect is detected in the NCI plots for some of the other systems studied.

3.4 Molecular trends: dispersion contributions and non-covalent interaction plots

The complete set of adsorption energies for the six small aromatic molecules with the three noble-metal surfaces is collected in Table 4, together with the XDM-dispersion and base-functional contributions. The dispersion contribution to the adsorption energies generally decreases down the group of coinage metals. Also, this energy decomposition shows that adsorption is entirely due to dispersion interactions, with the two exceptions of pyridine, in the perpendicular orientation, and 1,4-benzenediamine, where bonding between the molecular lone pair and the surface can result in a non-negligible contribution to binding from the base functional. However, the total adsorption energy, even in these two cases with incipient chemisorption behavior, is still dominated by the dispersion contribution. Lone pair–surface interactions will be discussed in detail throughout this section.

We now turn to the dependence of the absorption energies on molecular properties. We first consider the cases of benzene, furan, thiophene, and thiophenol, all of which prefer a parallel orientation to the surface such that dispersion interactions are maximized. The adsorption-energy trend for this series is furan < benzene < thiophene < thiophenol, which can be attributed to increasing molecular size and polarizability. Additionally, the heteroatom lone pairs become softer across this series due to greater polarizabililty of sulfur in the thiols than oxygen and the change from an sp^2 sulfur in thiophene to an sp^3 sulfur in thiophenol.

Experimentally, benzene and furan have been found to bind parallel to the surface,[5,65,66] in agreement with our calculations. However, thiophene and thiophenol have coverage-dependent surface orientations. At low coverages, both molecules prefer a parallel surface

Table 4: Calculated adsorption energies of selected molecules on the copper, silver, and gold surfaces, in eV. The contributions to the adsorption energies from the XDM dispersion correction and the base functional are also reported.

Molecule	Total			XDM			Base functional		
	Cu	Ag	Au	Cu	Ag	Au	Cu	Ag	Au
Benzene	0.59	0.68	0.64	1.01	0.85	0.75	-0.42	-0.17	-0.11
Furan	0.53	0.52	0.51	0.72	0.63	0.56	-0.19	-0.12	-0.05
Furan perp.	0.24	0.25	0.22	0.31	0.33	0.29	-0.08	-0.08	-0.07
Thiophene	0.66	0.67	0.62	0.90	0.77	0.69	-0.24	-0.11	-0.07
Thiophene perp.	0.40	0.40	0.25	0.49	0.47	0.32	-0.08	-0.07	-0.07
Thiophenol	1.00	0.90	0.91	1.15	1.05	0.90	-0.16	-0.15	0.01
Thiophenol perp.	0.35	0.36	0.33	0.44	0.39	0.34	-0.09	-0.03	-0.01
Pyridine	0.69	0.58	0.60	0.83	0.81	0.70	-0.14	-0.23	-0.09
Pyridine perp.	0.86	0.66	0.64	0.55	0.49	0.46	0.32	0.17	0.19
1,4-BDA (cis)	1.17	1.04	1.10	1.17	1.15	0.98	-0.01	-0.11	0.13
1,4-BDA (trans)	1.24	1.09	1.12	1.18	1.13	0.96	0.06	-0.04	0.16

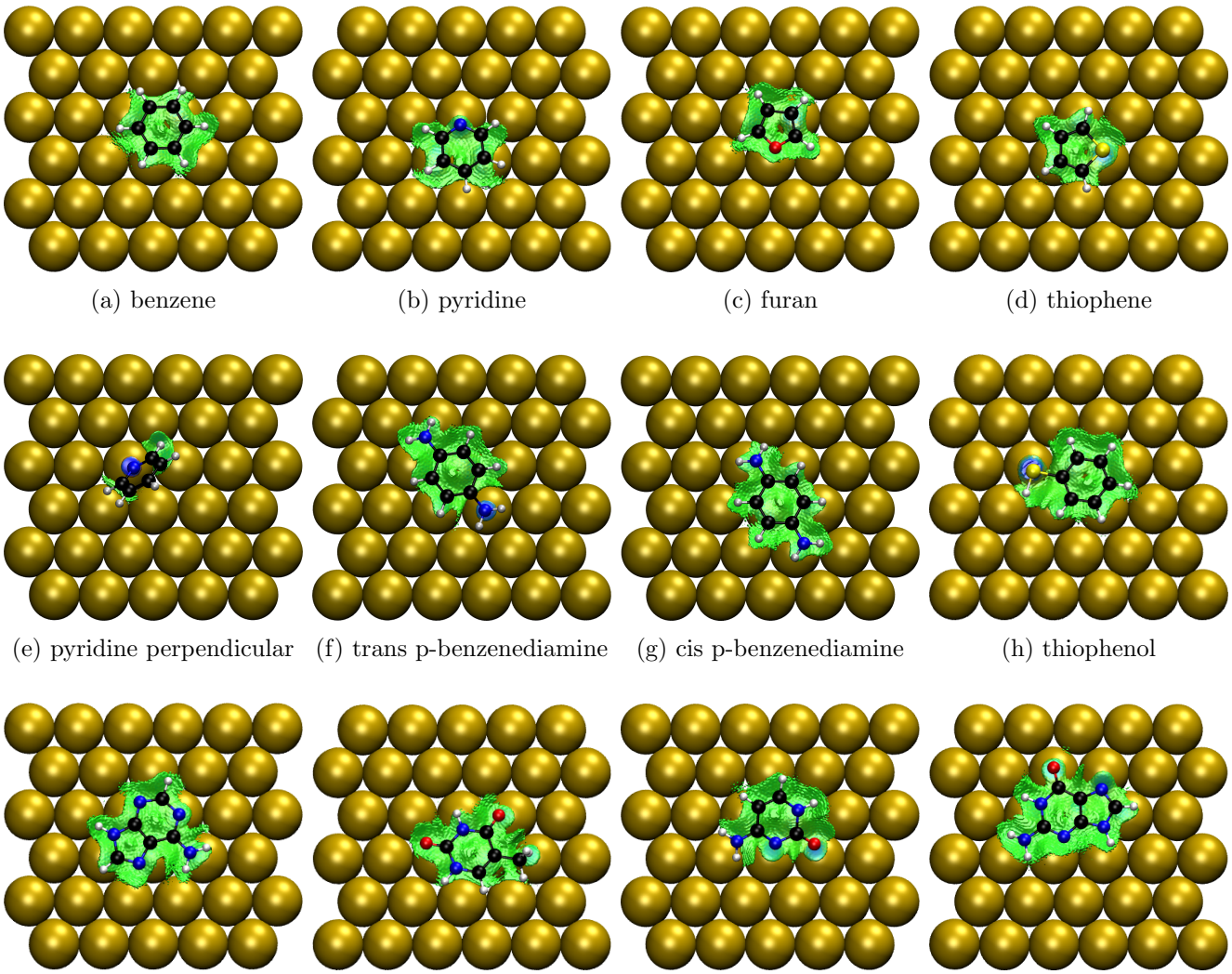

(a) benzene (b) pyridine (c) furan (d) thiophene

(e) pyridine perpendicular (f) trans p-benzenediamine (g) cis p-benzenediamine (h) thiophenol

(i) adenine (j) thymine (k) cytosine (l) guanine

Figure 1: NCI plots for selected molecules adsorbed on the gold surface using an $s = 0.6$ isosurface.

orientation, maximizing dispersion interactions between the aromatic ring and the surface, but as the coverage increases, thiophene and thiophenol adopt perpendicular orientations where sulfur-surface interactions dominate.[6,66–68] Our calculations (Table 4) predict that the parallel orientations are energetically preferred over the perpendicular orientations, in agreement with experimental observations. However, the perpendicular orientations of thiophene and thiophenol are still energetically favorable, and the stabilization during monolayer formation can be attributed to the additional dispersion interactions between the adjacent π-stacked molecules and to the monolayer being more densely packed if the molecules are perpendicular to the surface.

NCI plots, shown in Figure 1 for the gold surfaces, provide additional insight into the nature of the molecule-surface interactions. Broad green isosurfaces in the NCI plots correspond to dispersion interactions between the aromatic ring and the surface. The plots clearly show that dispersion interactions are dominant, in agreement with the adsorption-energy decomposition in Table 4. Additionally, the increased binding for softer lone pairs can be clearly seen in the coloring of the NCI plots. For thiophene, the NCI surface directly under the sulfur lone pair is light blue, indicating a slight increase in interaction strength. For thiophenol, the bluer region of the NCI plot shows that the sulfur interacts with the surface even more strongly, reflecting the greater adsorption energy. This is consistent with the known strong adsorption of thiophenol to gold in self-assembled monolayers.[69,70] While the NCI plots show favorable interactions between the sulfur atoms and the surface, they are not strong enough to significantly tilt the molecules, which form angles of 7° or less with the surface in the parallel orientation. The adsorption geometries (distances and angles between the aromatic ring and the surface) are given in the supporting information.

Like thiophene and thiophenol, pyridine's orientation on metal surfaces is coverage dependent.[10] At low coverages, pyridine prefers a parallel orientation where dispersion interactions dominate. As coverage increases, pyridine adopts a perpendicular orientation, interacting with the surface via the nitrogen lone pair and the monolayer is further is stabilized by π-stacking.[10] In the parallel orientation, pyridine has an adsorption energy similar to benzene (see Table 4), which is dominated by dispersion. However, interactions between the nitrogen atom and the surface cause the molecule to tilt slightly.[71] The tilt angle is largest for the copper surface and is 24°, compared to 13° and 9° for Ag and Au, respectively. In the perpendicular orientation, the NCI plot shows the loss of dispersion interactions between the surface and the pyridine π-system and an increased interaction between the surface and nitrogen. Perpendicular pyridine has the largest density in the NCI regions of all the molecules considered here. Indeed, perpendicular pyridine is one of only two molecules predicted to adsorb on the surface by the base functional alone and the interaction energy is greatest for copper.

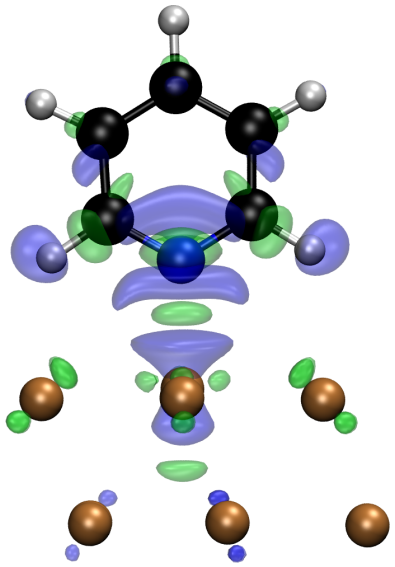

Figure 2: The polarization density for the physisorption of pyridine on a copper surface in the perpendicular orientation. The green iso-surface indicates and accumulation and the blue iso-surface depletion in electron density, for the adsorbed species relative to the separated molecule and surface at fixed geometries. The dipole of pyridine polarizes the surface, which induces further polarization of the nitrogen lone pair. This iso-density value is 0.016 a.u.

A plot of the polarization density, defined as the difference in electron density between the adsorbate and the isolated molecule and surface at fixed geometries, is shown for pyridine on the copper surface in Figure 2. In the perpendicular orientation, the dipole moment of pyridine is pointed directly down, towards the surface. This dipole polarizes the copper surface locally, inducing further polarization of the adsorbed pyridine. The strength of this interaction for the silver and gold surfaces is found to be roughly equal to the extent of dispersion stabilization, such that the adsorption energies for perpendicular and parallel orientations are effectively equal. However, the results show that the perpendicular orientation of pyridine is favored for copper, where pyridine approaches the surface more closely. In this case, the induced electrostatic interactions become more favorable, as seen from the larger adsorption-energy contribution from the base functional (Table 4).

As discussed in the preceding section, 1,4-benzenediamine can adsorb as either a *cis* or *trans* isomer. Our results predict that the *cis* isomer has a weaker adsorption energy than the *trans* isomer. Adsorption of the *cis* isomer is entirely due to dispersion; it lies flat, with a near zero tilt angle and the amine hydrogens pointing down, towards the surface. As for perpendicular pyridine, a strong nitrogen-metal interaction appears in the NCI plot for the *trans* isomer and this results in a slightly tilted orientation on the surface with angles of 7-8°. Calculated adsorption energies for the *trans* isomer of BDA are approximately the sum of both perpendicular and parallel pyridine adsorption energies. The adsorption motif of *trans* BDA suggests that the *cis* isomer may adsorb more strongly if both nitrogen lone pairs were directed towards the surface, instead of away from it, as shown in Figure 1. However, the *trans* isomer experiences significant polarization, which is not possible in the *cis* isomer if both nitrogen lone pairs are directed towards the surface.

3.5 Nucleobases

Calculated adsorption energies for the nucleobases on the metal surfaces are given in Table 5. Our results show that adsorption is primarily driven by dispersion interactions. The dispersion energies follow the order cytosine < thymine < adenine < guanine, with greater molecular size leading to increased dispersion attraction. Adenine has a flat surface orientation since the nitrogen lone pairs all conjugate with the π-system and have little direct interaction with the surface. Thymine has a slightly tilted geometry for copper and silver surfaces, but lies almost flat on gold, in agreement with STM images.[74,75] Conversely, cytosine and guanine adopt tilted geometries, at angles of 12-14° to the gold surface, each with the C=O group pointing slightly downward.

The NCI plots in Figure 1 offer a picture consistent with the adsorption geometries, showing that the oxygen atoms interact fairly strongly with the surface, in an analogous fashion to our results for *trans* 1,4-benzenediamine. Favorable interactions between the C=O groups and the surface also result in less repulsion from the base functional and the total adsorption energies follow the trend thymine < cytosine < adenine < guanine, though the ordering of cytosine and adenine are reversed for copper due to a stronger interaction of the oxygen atoms with this surface.

The calculated nucleobase adsorption energies are compared with experimental TPD adsorption for gold surfaces in Table 6. The computed adsorption energies are roughly half of those reported experimentally.[72,73] This is because the calculated energies correspond to the adsorption of a single, isolated molecule on the surface and lack the intermolecular interactions between adjacent nucleobases that are reflected in experiment, specifically hydrogen bonding. The experimental determination of single-molecule adsorption energies for nucleobases is difficult because of the formation of strong intermolecular hydrogen-bonds leading to the formation of molecular lines and clusters on metal surfaces, even at low coverages.[72] Since the TPD adsorption energies are measured for higher coverages, they contain contributions from intermolecular interactions within the monolayer[72,73,76–80] that must be included in the theoretical treatment as well. Note that

Table 5: Calculated nucleobase adsorption energies for the copper, silver, and gold surfaces, in eV/molecule. The contributions to the total adsorption energies from the XDM dispersion correction and the base functional are also reported.

Molecule	Total			XDM			Base functional		
	Cu	Ag	Au	Cu	Ag	Au	Cu	Ag	Au
Guanine	1.07	1.03	0.94	1.22	1.14	1.00	-0.15	-0.11	-0.06
Cytosine	0.96	0.90	0.77	0.91	0.88	0.79	0.05	0.02	-0.02
Adenine	0.83	0.86	0.81	1.08	1.04	0.91	-0.25	-0.18	-0.10
Thymine	0.67	0.69	0.67	0.91	0.92	0.79	-0.24	-0.24	-0.12

Table 6: Comparison of calculated and experimental TPD adsorption energies for the nucleobases on the gold surface, in eV/molecule. The contribution of intermolecular hydrogen bonding is shown for both an estimated additive correction (Est.) and from the results of calculations on small nucleobase clusters (Calc.). The total DFT adsorption energies correspond to the sum of the single-molecule adsorption energies and these hydrogen-bond corrections.

Molecule	Surface	H-Bond		Total		Expt.
		Est.	Calc.	Est.	Calc.	
Guanine	0.94	0.86	0.84	1.80	1.78	1.44,[72] 1.51[73]
Cytosine	0.77	0.65	0.73	1.42	1.50	1.26,[72] 1.35[73]
Adenine	0.81	0.65	0.60	1.46	1.41	1.41,[72] 1.36[73]
Thymine	0.67	0.43	0.53	1.10	1.20	1.08,[72] 1.15[73]

these experimental values are also expected to have fairly large uncertainties given the high coverage sensitivity of Redhead analysis.[36]

To properly account for intermolecular hydrogen-bonding effects, periodic-boundary DFT calculations should be performed on a complete adsorbed monolayer. However, this presents considerable practical difficulty since the cell lengths corresponding to the monolayer and metal surface are not necessarily commensurate. Thus, to approximately account for intermolecular hydrogen-bonding, it was assumed that all possible donor and acceptor sites on the nucleobases would participate in hydrogen bonding, with an average strength of 0.22 eV (5 kcal/mol). Since two molecules are needed to form each hydrogen bond, this results in an energetic contribution of 0.11 eV (2.5 kcal/mol) per hydrogen-bond per molecule. The estimated hydrogen-bonding contributions are given in Table 6, considering that the four nucleobases can form four (thymine), six (cytosine and adenine), and eight (guanine) hydrogen bonds in total. Naturally, this is a rough estimate, but it serves to illustrate the origin of the missing stabilizing contribution.

As an alternative, approximate hydrogen-bond energies were also computed using the small nucleobase clusters whose structure is shown in the supporting information. These structures were chosen to match previous STM/DFT studies.[74,77,78,80] The calculations were performed with Gaussian09[81] using the LC-ωPBE[82,83] functional, XDM dispersion,[38] and the pc-2-spd basis set.[84] The results are given in Table 6 and show that the calculated and estimated hydrogen-bond contributions are in good agreement, and are generally on the same order as the single-molecule adsorption energies. Adding either of these hydrogen-bonding corrections gives total physisorption energies that are in good agreement with the experimental TPD values.[72,73]

4 Summary

This work investigated the ability of the XDM dispersion model to predict surface adsorption energies. Adsorption energies for a collection of molecules (benzene, furan, pyridine, thiophene, thiophenol, benzenediamine, and the four DNA nucleobases) on the (111) surfaces of coinage metals were calculated using the B86bPBE-XDM functional.

The adsorption energies are found to be dominated by dispersion interactions and increase with molecular size. Inclusion of polarizable heteroatoms also tends to increase the adsorption energies and leads to a preferential molecular adsorption orientation (e.g. perpendicular). The non-covalent interaction (NCI) plot technique was applied to probe the nature of the molecule-surface binding in real space. In general, NCI reveals incipient chemisorption contributions in cases where a molecular lone pair interacts with the surface and there is an increased binding contribution from the base density functional.

The calculated adsorption energies are in excellent agreement with experimental best-estimates for benzene on the various metal surfaces, with an mean average error (MAE) of 0.04 eV, which is comparable to the experimental precision. The MAE from similar dispersion-corrected functionals for benzene on the three metal surfaces is 0.19 (PBE-D3), 0.20–0.25 (PBE-TS), 0.08–0.11 (PBE-TS$^{\text{surf}}$), $0.04 - 0.08$ for MBD, and a range of $0.03 - 0.15$ eV from several vdw-DF functionals.

Our results dispel previous doubts about whether pairwise dispersion corrections can be used for the modeling of surface adsorptions. Contrary to previous applications of XDM and in contrast to PBE-TS$^{\text{surf}}$, physisorption can be reliably modeled with the canonical implementation of XDM combined with the usual B86bPBE base functional, which is known to give very accurate results for intermolecular interactions. Hence, B86bPBE-XDM should be a promising approach to model chemical processes occurring on material surfaces, with a cost comparable to any semilocal density functional.

Supporting Information Available: Tables of optimized unit-cell dimensions for the bulk metals; molecule-surface distances and angles for physisorbed species; convergence of the adsorption energy for trans 1,4-benzenediamine on copper with respect to **k**-points, plane-wave cut-offs, and surface thickness; and adsorption energy comparison depending on the unit-cell dimensions for the isolated molecules. Figure of the gas-phase clusters used to estimate the hydrogen-bonding contribution to the experimental adsorption energies in the four nucleobases. Quantum ESPRESSO files showing the final relaxed geometries and energies for all species are also given. This material is available free of charge via the Internet at `http://pubs.acs.org/`.

Acknowledgement MSC thanks XSEDE, ERJ thanks Compute Canada and Westgrid, and AOR thanks the Spanish Malta/Consolider initiative, number CSD2007-00045, for computational resources. ERJ thanks the National Science and Engineering Research Council of Canada (NSERC) for financial support.

References

(1) Tsukruk, V. V.; Rinderspacher, F.; Bliznyuk, V. N. Self-Assembled Multilayer Films from Dendrimers. *Langmuir* **1997**, *13*, 2171–2176.

(2) Heath, J. R. Molecular Electronics. *Annu. Rev. Mater. Res.* **2009**, *39*, 1–23.

(3) Scott, J. C. MetalÄìorganic interface and charge injection in organic electronic devices. *Journal of Vacuum Science & Technology A* **2003**, *21*, 521–531.

(4) Johánek, V.; Schauermann, S.; Laurin, M.; Gopinath, C. S.; Libuda, J.; Freund, H.-J. On the Role of Different Adsorption and Reaction Sites on Supported Nanoparticles during a Catalytic Reaction:? NO Decomposition on a Pd/Alumina Model Catalyst. *J. Phys. Chem. B* **2004**, *108*, 14244–14254.

(5) Xi, M.; Yang, M. X.; Jo, S. K.; Bent, B. E.; Stevens, P. Benzene adsorption on Cu(111): Formation of a stable bilayer. *J. Chem. Phys.* **1994**, *101*, 9122–9131.

(6) Milligan, P. K.; Murphy, B.; Lennon, D.; Cowie, B. C. C.; Kadodwala, M. A Complete Structural Study of the Coverage Dependence of the Bonding of Thiophene on Cu(111). *J. Phys. Chem. B* **2001**, *105*, 140–148.

(7) Väterlein, P. et al. Orientation and bonding of thiophene and 2,2-bithiophene on Ag(111): a combined near edge extended X-ray absorption fine structure and X scattered-wave study. *Surf. Sci.* **2000**, *452*, 20–32.

(8) Liu, G.; Rodriguez, J. A.; Dvorak, J.; Hrbek, J.; Jirsak, T. Chemistry of sulfur-containing molecules on Au: thiophene, sulfur dioxide, and methanethiol adsorption. *Surf. Sci.* **2002**, *505*, 295–307.

(9) Mulligan, A.; Johnston, S. M.; Miller, G.; Dhanak, V.; Kadodwala, M. A TPD and NIXSW investigation of furan and tetrahydrofuran adsorption on Cu(111). *Surf. Sci.* **2003**, *541*, 3–13.

(10) Zhong, Q.; Gahl, C.; Wolf, M. Two-photon photoemission spectroscopy of pyridine adsorbed on Cu. *Surf. Sci.* **2002**, *496*, 21–32.

(11) Dell'Angela, M. et al. Relating Energy Level Alignment and Amine-Linked Single Molecule Junction Conductance. *Nano Lett.* **2010**, *10*, 2470–2474.

(12) Tkatchenko, A.; Romaner, L.; Hofmann, O. T.; Zojer, E.; Ambrosch-Draxl, C.; Scheffler, M. Van der Waals interactions between organic adsorbates and at organic/inorganic interfaces. *MRS Bull.* **2010**, *35*, 435–442.

(13) Liu, W.; Tkatchenko, A.; Scheffler, M. Modeling Adsorption and Reactions of Organic Molecules at Metal Surfaces. *Acc. Chem. Res.* **2014**, *47*, 3369 – 3377.

(14) Reimers, J. R. et al. A priori calculations of the free energy of formation from solution of polymorphic self-assembled monolayers. *Proc. Nat. Acad. Sci.* **2015**, *112*, E6101–E6110.

(15) Reimers, J. R. et al. From chaos to order: Chain-length dependence of the free energy of formation of meso-tetraalkylporphyrin self-assembled monolayer polymorphs. *J. Phys. Chem. C* **2016**, *120*, 1739–1748.

(16) Johnson, E. R.; Mackie, I. D.; DiLabio, G. A. Dispersion interactions in density-functional theory. *J. Phys. Org. Chem.* **2009**, *22*, 1127.

(17) DiLabio, G. A.; Otero-de-la Roza, A. Dispersion Interactions in Density-Functional Theory. *Rev. Comp. Chem.* **2014**, arXiv:1405.1771.

(18) Bilic, A.; Reimers, J. R.; Hush, N. S.; Hoft, R. C.; Ford, M. J. Adsorption of Benzene on Copper, Silver, and Gold Surfaces. *J. Chem. Theory Comput.* **2006**, *2*, 1093–1105.

(19) Ferrighi, L.; Madsen, G. K. H.; Hammer, B. Self-consistent meta-generalized gradient approximation study of adsorption of aromatic molecules on noble metal surfaces. *J. Chem. Phys.* **2011**, *135*, 084704.

(20) Callsen, M.; Atodiresei, N.; Caciuc, V.; Blügel, S. Semiempirical van der Waals interactions versus ab initio nonlocal correlation effects in the thiophene-Cu(111) system. *Phys. Rev. B* **2012**, *86*, 085439.

(21) Tonigold, K.; Gross, A. Adsorption of small aromatic molecules on the (111) surfaces of noble metals: A density functional theory study with semiempirical corrections for dispersion effects. *J. Chem. Phys.* **2010**, *132*, 224701.

(22) Grimme, S.; Antony, J.; Ehrlich, S.; Krieg, H. A consistent and accurate ab initio parametrization of density functional dispersion correction (DFT-D) for the 94 elements H-Pu. *J. Chem. Phys.* **2010**, *132*, 154104.

(23) Reckien, W.; Eggers, M.; Bredow, T. Theoretical study of the adsorption of benzene on coinage metals. *Beilstein J. Org. Chem.* **2014**, *10*, 1775–1784.

(24) Chwee, T. S.; Sullivan, M. B. Adsorption studies of C6H6 on Cu (111), Ag (111), and Au (111) within dispersion corrected density functional theory. *J. Chem. Phys.* **2012**, *137*, 134703.

(25) Liu, W. et al. Structure and energetics of benzene adsorbed on transition-metal surfaces: density-functional theory with van der Waals interactions including collective substrate response. *New J. Phys.* **2013**, *15*, 053046.

(26) Liu, W.; Carrasco, J.; Santra, B.; Michaelides, A.; Scheffler, M.; Tkatchenko, A. Benzene adsorbed on metals: Concerted effect of covalency and van der Waals bonding. *Phys. Rev. B* **2012**, *86*, 245405.

(27) Ruiz, V. G.; Liu, W.; Zojer, E.; Scheffler, M.; Tkatchenko, A. Density-Functional Theory with Screened van der Waals Interactions for the Modeling of Hybrid Inorganic-Organic Systems. *Phys. Rev. Lett.* **2012**, *108*, 146103.

(28) Carrasco, J.; Liu, W.; Michaelides, A.; Tkatchenko, A. Insight into the description of van der Waals forces for benzene adsorption on transition metal (111) surfaces. *J. Chem. Phys.* **2014**, *140*, 084704.

(29) Liu, W. et al. Quantitative Prediction of Molecular Adsorption: Structure and Binding of Benzene on Coinage Metals. *Phys. Rev. Lett.* **2015**, *115*, 036104.

(30) Yildirim, H.; Greber, T.; Kara, A. Trends in Adsorption Characteristics of Benzene on Transition Metal Surfaces: Role of Surface Chemistry and van der Waals Interactions. *J. Phys. Chem. C* **2013**, *117*, 20572–20583.

(31) Silvestrelli, P. L.; Ambrosetti, A. Inclusion of screening effects in the van der Waals corrected DFT simulation of adsorption processes on metal surfaces. *Phys. Rev. B* **2013**, *87*, 075401.

(32) Carter, D.; Rohl, A. L. van der Waals Corrected Density Functional Calculations of the Adsoprtion of Benzene on the Cu (111) Surface. *J. Comp. Chem.* **2014**, *35*, 2263–2271.

(33) Peng, H.; Yang, Z.-H.; Sun, J.; Perdew, J. P. SCAN+rVV10: A promising van der Waals density functional. **2015**, http://arxiv.org/pdf/1510.05712v1.pdf.

(34) Redhead, P. Thermal desorption of gases. *Vacuum* **1962**, *12*, 203–211.

(35) de Jong, A.; Niemantsverdriet, J. Thermal desorption analysis: Comparative test of ten commonly applied procedures. *Surf. Sci.* **1990**, *233*, 355–365.

(36) Nieskens, D.; van Bavel, A.; Niemantsverdriet, J. The analysis of temperature programmed desorption experiments of systems with lateral interactions; implications of the compensation effect. *Surf. Sci.* **2003**, *546*, 159–169.

(37) Becke, A. D.; Johnson, E. R. Exchange-hole dipole moment and the dispersion interaction revisited. *J. Chem. Phys.* **2007**, *127*, 154108.

(38) Otero de la Roza, A.; Johnson, E. R. Noncovalent interactions and thermochemistry using XDM-corrected hybrid and range-separated hybrid density functionals. *J. Chem. Phys.* **2013**, *138*.

(39) Otero de la Roza, A.; Johnson, E. R. A benchmark for non-covalent interactions in solids. *J. Chem. Phys.* **2012**, *137*, 054103.

(40) Otero de la Roza, A.; Johnson, E. R. Van der Waals interactions in solids using the exchange-hole dipole moment. *J. Chem. Phys.* **2012**, *136*, 174109.

(41) Otero de la Roza, A.; Mallory, J. D.; Johnson, E. R. Metallophilic interactions from dispersion-corrected density-functional theory. *J. Chem. Phys.* **2014**, *140*, 18A504.

(42) Johnson, E. R.; Becke, A. D. A post-Hartree-Fock model of intermolecular interactions: Inclusion of higher-order corrections. *J. Chem. Phys.* **2006**, *124*, 174104.

(43) Johnson, E. R.; Keinan, S.; Mori-Sánchez, P.; Contreras-García, J.; Cohen, A. J.; Yang, W. Revealing Noncovalent Interactions. *J. Am. Chem. Soc.* **2010**, *132*, 6498–6506.

(44) Otero de la Roza, A.; Johnson, E. R.; Contreras-Garcia, J. Revealing non-covalent interactions in solids: NCI plots revisited. *Phys. Chem. Chem. Phys.* **2012**, *14*, 12165–12172.

(45) Blöchl, P. E. Projector augmented-wave method. *Phys. Rev. B* **1994**, *50*, 17953.

(46) Giannozzi, P.; Baroni, S.; et. al., QUANTUM ESPRESSO: a modular and open-source software project for quantum simulations of materials. *J. Phys. Condens. Mat.* **2009**, *21*, 395502.

(47) Becke, A. D. On the large?gradient behavior of the density functional exchange energy. *J. Chem. Phys.* **1986**, *85*, 7184–7187.

(48) Perdew, J. P.; Burke, K.; Ernzerhof, M. Generalized gradient approximation made simple. *Phys. Rev. Lett.* **1996**, *77*, 3865.

(49) Marzari, N.; Vanderbilt, D.; De Vita, A.; Payne, M. C. Thermal Contraction and Disordering of the Al(110) Surface. *Phys. Rev. Lett.* **1999**, *82*, 3296–3299.

(50) Otero de la Roza, A.; Johnson, E. R.; Luaña, V. Critic2: A program for real-space analysis of quantum chemical interactions in solids. *Comput. Phys. Commun.* **2014**, *185*, 1007–1018.

(51) Hansen, A.; Bannwarth, C.; Grimme, S.; Petrović, P.; Werlé, C.; Djukic, J.-P. The thermochemistry of London dispersion-driven transition metal reactions: Getting the right answer for the right reason. *ChemistryOpen* **2014**, *3*, 177–189.

(52) Tkatchenko, A.; Scheffler, M. Accurate Molecular Van Der Waals Interactions from Ground-State Electron Density and Free-Atom Reference Data. *Phys. Rev. Lett.* **2009**, *102*, 073005.

(53) Zaremba, E.; Kohn, W. Van der Waals interaction between an atom and a solid surface. *Phys. Rev. B* **1976**, *13*, 2270 – 2285.

(54) Tkatchenko, A.; DiStasio, R. A.; Car, R.; Scheffler, M. Accurate and Efficient Method for Many-Body van der Waals Interactions. *Phys. Rev. Lett.* **2012**, *108*, 236402.

(55) Ambrosetti, A.; Reilly, A. M.; DiStasio, R. A.; Tkatchenko, A. Long-range correlation energy calculated from coupled atomic response functions. *J. Chem. Phys.* **2014**, *140*, 18A508.

(56) Dion, M.; Rydberg, H.; Schröder, E.; Langreth, D. C.; Lundqvist, B. I. Van der Waals density functional for general geometries. *Phys. Rev. Lett.* **2004**, *92*, 246401.

(57) Lee, K.; Murray, É. D.; Kong, L.; Lundqvist, B. I.; Langreth, D. C. Higher-accuracy van der Waals density functional. *Phys. Rev. B* **2010**, *82*, 081101.

(58) Lacks, D. J.; Gordon, R. G. Pair interactions of rare-gas atoms as a test of exchange-energy-density functionals in regions of large density gradients. *Phys. Rev. A* **1993**, *47*, 4681.

(59) Hirshfeld, F. L. Bonded-atom fragments for describing molecular charge densities. *Theor. Chim. Acta* **1977**, *44*, 129–138.

(60) Becke, A. D.; Roussel, M. R. Exchange holes in inhomogeneous systems: A coordinate-space model. *Phys. Rev. A* **1989**, *39*, 3761–3767.

(61) Becke, A. D.; Johnson, E. R. Exchange-hole dipole moment and the dispersion interaction: High-order dispersion coefficients. *J. Chem. Phys.* **2006**, *124*, 014104.

(62) Johnson, E. R. Dependence of dispersion coefficients on atomic environment. *J. Chem. Phys.* **2011**, *135*, 234109.

(63) Mori-Sánchez, P.; Martín Pendás, A.; Luaña, V. A classification of covalent, ionic, and metallic solids based on the electron density. *J. Am. Chem. Soc.* **2002**, *124*, 14721–14723.

(64) Li, G.; Tamblyn, I.; Cooper, V. R.; Gao, H.-J.; Neaton, J. B. Molecular adsorption on metal surfaces with van der Waals density functionals. *Phys. Rev. B* **2012**, *85*, 121409.

(65) Zhou, X.-L.; Castro, M.; White, J. Interactions of UV photons and low energy electrons with chemisorbed benzene on Ag(111). *Surf. Sci.* **1990**, *238*, 215–225.

(66) Sexton, B. *Surf. Sci.* **1985**, *163*, 99–113.

(67) Milligan, P.; McNamarra, J.; Murphy, B.; Cowie, B.; Lennon, D.; Kadodwala, M. A {NIXSW} and {NEXAFS} investigation of thiophene on Cu(111). *Surf. Sci.* **1998**, *412-413*, 166–173.

(68) Barnes, C. J.; Whelan, C. M.; Gregoire, C.; Pireaux, J.-J. A HREELS STUDY OF BENZENETHIOL ADSORPTION ON Au(111) AND Au(322). *Surf. Rev. Lett.* **1999**, *06*, 193–203.

(69) Schreiber, F. Structure and growth of self-assembling monolayers. *Prog. Surf. Sci.* **2000**, *65*, 151–256.

(70) Carron, K. T.; Hurley, L. G. Axial and azimuthal angle determination with surface-enhanced Raman spectroscopy: thiophenol on copper, silver, and gold metal surfaces. *J. Phys. Chem.* **1991**, *95*, 9979–9984.

(71) Avouris, P.; Demuth, J. E. Electronic excitations of benzene, pyridine, and pyrazine adsorbed on Ag(111). *J. Chem. Phys.* **1981**, *75*, 4783–4794.

(72) Östblom, M.; Liedberg, B.; Demers, L. M.; Mirkin, C. A. On the Structure and Desorption Dynamics of DNA Bases Adsorbed on Gold: A Temperature-Programmed Study. *J. Phys. Chem. B* **2005**, *109*, 15150–15160.

(73) Demers, L. M.; Östblom, M.; Zhang, H.; Jang, N.-H.; Liedberg, B.; Mirkin, C. A. Thermal Desorption Behavior and Binding Properties of DNA Bases and Nucleosides on Gold. *J. Am. Chem. Soc.* **2002**, *124*, 11248–11249.

(74) Xu, W. e. a. Probing the HIerachy of Thymine-Thymine INteractions in Self-Assembled Structures by Manipulation with Scanning Tunneling MIcrscopy. *Small* **2007**, *3*, 2011–2014.

(75) Roelfs, B. et al. Adsorption of Thymine on Gold Single-Crystal Electrodes. *J. Phys. Chem. B* **1997**, *101*, 754–765.

(76) Tao, N. J.; DeRose, J. A.; Lindsay, S. M. Self-assembly of molecular superstructures studied by in situ scanning tunneling microscopy: DNA bases on gold (111). *J. Phys. Chem.* **1993**, *97*, 910–919.

(77) Otero, R. et al. Elementary Structural Motifs in a Random Network of Cytosine

Adsorbed on a Gold(111) Surface. *Science* **2008**, *319*, 312–315.

(78) Kelly, R. E. An Investigation into the Interactions Between Self-Assembled Adenine Molecules and a Au(111) Surface. *Small* **2008**, *4*, 1494–1500.

(79) Furukawa, M.; Tanaka, H.; Kawai, T. The role of dimer formation in the self-assemblies of DNA bas molecules on Cu(111) surfaces: A scanning tunneling microscope study. *J. Chem. Phys.* **2001**, *115*, 3419–3423.

(80) Otero, R. et al. Guanine Quartet Networks Stabilized by Cooperative Hydrogen Bonds. *Angew. Chem. Int. Ed.* **2005**, *44*, 2270–2275.

(81) Frisch, M. J. et al. Gaussian 09 Revision A.1. Gaussian Inc. Wallingford CT 2009.

(82) Vydrov, O. A.; Scuseria, G. E. Assessment of a long-range corrected hybrid functional. *J. Chem. Phys.* **2006**, *125*, 234109.

(83) Vydrov, O. A.; Heyd, J.; Krukau, A. V.; Scuseria, G. E. Importance of short-range versus long-range Hartree-Fock exchange for the performance of hybrid density functionals. *J. Chem. Phys.* **2006**, *125*, 074106.

(84) Johnson, E. R.; Otero-de-la Roza, A.; Dale, S. G.; DiLabio, G. A. Efficient basis sets for non-covalent interactions in XDM-corrected density-functional theory. *J. Chem. Phys.* **2013**, *139*, 214109.

Graphical TOC Entry

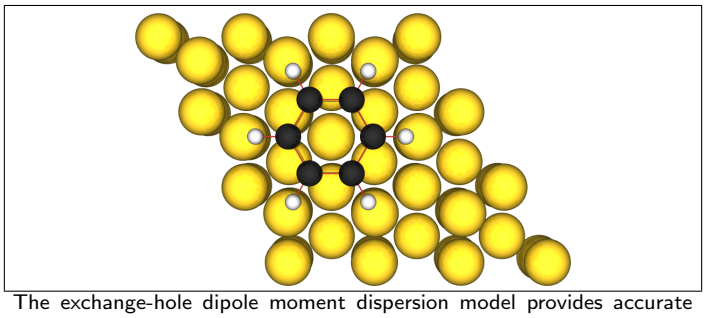

The exchange-hole dipole moment dispersion model provides accurate results for molecular physisorption on coinage-metal surfaces. This performance is achieved without changes to the canonical implementation of the XDM method, making it an excellent candidate for studying chemistry on a material surface.